Polyhedron 151 (2018) 446–451

Contents lists available at ScienceDirect

Polyhedron

journal homepage: www.elsevier.com/locate/poly

Directed synthesis and magnetic properties of a hexanuclear ferric cluster

Jeff Lengyel [a], Sebastian A. Stoian [b,*], Naresh Dalal [a], Michael Shatruk [a,*]

[a] Department of Chemistry and Biochemistry, Florida State University, 95 Chieftan Way, Tallahassee, FL 32306, USA
[b] Department of Chemistry, University of Idaho, 875 Perimeter Dr, Moscow, ID 83844, USA

ARTICLE INFO

Article history:
Received 14 April 2018
Accepted 1 June 2018
Available online 15 June 2018

Keywords:
Ferric complexes
Clusters
Spin frustration
Antiferromagnetic exchange
Coordination chemistry

ABSTRACT

The hexanuclear iron(III) complex, $[Fe_6(\mu_3\text{-}3\text{-bpp})_4(\mu_3\text{-}O)_2(\mu_2\text{-}OMe)_{3.67}(\mu_2\text{-}OH)_{0.33}Cl_2]\cdot 0.33MeOH\cdot H_2O$ (**1**) was synthesized by a redox reaction between $FeCl_2$, $AgNO_2$, and 3-H_2bpp in methanol (3-H_2bpp = 2,6-bis(3-pyrazolyl)pyridine). The crystal structure of the complex is composed of two trinuclear subunits related by an inversion operation. This symmetry results in an overall octahedral arrangement of Fe(III) sites within the cluster. The four equatorial Fe sites are linked together by μ_2-OMe^- and μ_2-OH^- bridges, while each of the four 3-bpp^{2-} bridges spans two axial and one equatorial Fe sites. The two Cl^- ligands cap the axial Fe sites. The difference in the coordination environment for the equatorial and axial Fe sites is validated by the observation of two quadrupole doublets in the Mössbauer spectrum of **1**, which also confirms that all metal sites correspond to the high-spin Fe(III) ions. Temperature-dependent magnetic susceptibility data reveal strong antiferromagnetic exchange coupling between the Fe(III) centers, which is also justified by quantum-chemical calculations at the density-functional level of theory.

1. Introduction

Oxo-bridged ferric complexes have been studied extensively vis-à-vis their magnetic properties. In particular, a detailed analysis was performed by Gorun and Lippard to understand the correlation between interatomic distances in the core of the cluster and the strength of antiferromagnetic exchange coupling [1]. Somewhat later, complexes with ferro- or ferrimagnetic ground states have received renewed attention as potential single-molecule magnets (SMMs) [2–4]. In addition, multinuclear ferric complexes also play an important role as active sites in many metalloproteins [5]. The search for new SMMs has somewhat sidelined attention to ferric complexes with low total spin values, i.e. with antiferromagnetic ground states. Nevertheless, the frequent occurrence of trinuclear μ_3-oxo centered subunits in such complexes is fundamentally interesting, as it offers a fertile playground for testing simple models aimed at understanding how the balance between mutually conflicting antiferromagnetic coupling pathways (briefly, spin frustration) defines the ground spin state in such systems [6–8].

The synthesis of ferrous complexes with N-donating ligands represents an active area of research, due to the proclivity of such compounds to exhibit switching between the low-spin and high-spin electronic configurations (spin crossover) [9–11]. In the course of such studies, one sometimes encounters byproduct ferric complexes – the result of increased air sensitivity of the high-spin Fe(II) ion due to the population of the higher-energy antibonding e_g orbitals, which remain vacant in the low-spin Fe(II) ion. Typically, the yield of such byproducts is low or negligible, as one tries to avoid their formation by careful handling of reaction mixtures under air-free conditions. Occasionally, however, a ferric byproduct might be an unavoidable outcome caused by circumstances accompanying the reaction.

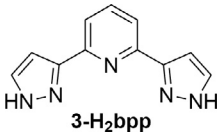

3-H_2bpp

Our interest in certain N-donating ligands that consistently lead to the formation of Fe(II) complexes with abrupt spin transitions, which may be accompanied by crystallographic symmetry breaking [12], led us to investigate the preparation of salts of the

* Corresponding authors.
E-mail addresses: sstoian@uidaho.edu (S.A. Stoian), shatruk@chem.fsu.edu (M. Shatruk).

https://doi.org/10.1016/j.poly.2018.06.004
0277-5387/

well-known spin-crossover cation, $[Fe(3\text{-}H_2bpp)_2]^{2+}$, where 3-$H_2$bpp = 2,6-bis(3-pyrazolyl)pyridine [13–15]. In the course of these studies, we discovered the formation of an interesting hexanuclear Fe(III) cluster due to the oxidation of the Fe(II) centers by NO_2^- ions. Attempts to synthesize such cluster in a direct manner, i.e. in the absence of NO_2^- as an oxidizing agent, failed, while the use of $AgNO_2$ in the reaction consistently led to the isolation of this product. Herein, we report the synthesis and crystal structure of this hexanuclear complex, $[Fe_6(\mu_3\text{-}3\text{-}bpp)_4(\mu_3\text{-}O)_2(\mu_2\text{-}OMe)_{3.67}(\mu_2\text{-}OH)_{0.33}Cl_2]\cdot 0.33MeOH\cdot H_2O$ (**1**), and provide a detailed analysis of its magnetic properties by a combination of magnetic measurements, Mössbauer spectroscopy, and density-functional theory (DFT) calculations.

2. Materials and methods

2.1. Synthesis

All reactions were performed under an inert N_2 atmosphere using standard Schlenk techniques. All reagents were purchased from Aldrich or Alfa Aesar, except for 3-H_2bpp, which was prepared according to the previously published procedure [16]. ACS grade methanol was purged with dry N_2 gas for 30 min prior to use. Elemental analysis was performed by Atlantic Microlab, Inc. (Norcross, GA, USA).

2.1.1. $[Fe_6(\mu_3\text{-}3\text{-}bpp)_4(\mu_3\text{-}O)_2(\mu_2\text{-}OMe)_{3.67}(\mu_2\text{-}OH)_{0.33}Cl_2]\cdot 0.33MeOH\cdot H_2O$ (**1**)

A 50-mL Schlenk flask was charged with 50 mg (0.25 mmol) of $FeCl_2\cdot 4H_2O$ and 210 mg (1.00 mmol) of 3-H_2bpp, and 20 mL of methanol was added with stirring to result in a clear gold-yellow solution. To this solution was added 230 mg (1.50 mmol) of $AgNO_2$, and the reaction mixture was stirred for 1 h. After this time, a black precipitate that formed was filtered off via cannula. The dark-orange solution obtained was allowed to slowly evaporate under a flow of N_2 gas or layered with anhydrous diethyl ether. In both cases, X-ray quality single crystals were obtained within a few days. The crystals were isolated by filtration, washed with cold MeOH, and dried under suction. Yield = 24 mg (41%). *Anal.* Calc. (Found) for $Fe_6Cl_2O_{7.66}N_{20}C_{48}H_{43.3}$ (**1**),%: C 41.3 (40.35), H 3.22 (3.06), N 18.8 (19.61).

2.1.2. X-Ray crystallography

Single-crystal X-ray diffraction was performed on a Bruker APEX-II diffractometer equipped with a CCD detector and a graphite-monochromated Mo Kα radiation source (λ = 0.71073 Å). A single crystal of **1** was suspended in Paratone-N oil (Hampton Research) and mounted on a cryoloop which was cooled to 100 K in an N_2 cold stream. The data set was recorded as ω-scans at 0.3° step width and integrated with the Bruker SAINT software package [17]. A multi-scan adsorption correction was applied based on multiple equivalent measurements (SADABS) [18]. The space group was determined with XPREP [19], and the crystal structure solution and refinement were carried out using the SHELX software [20]. The final refinement was performed with anisotropic atomic displacement parameters for all non-hydrogen atoms, except for the atoms that belonged to a disordered part of the structure. The latter included one of the bridging units (see the Crystal Structure section below), which was occupied either by methoxide or hydroxide group. The total occupancy of these groups was set to 1. Based on interatomic distances observed, a nearby methanol molecule was modeled as present when the bridge was occupied by μ_2-OH^- and absent when the bridge was occupied by μ_2-OMe^-. Such disorder model also led to more meaningful atomic displacement parameters for the non-hydrogen atoms. All H atoms were placed in calculated positions and refined in the riding model. Full details of the crystal structure refinement have been deposited with the Cambridge Crystallographic Data Centre (CCDC). A brief summary of data collection and refinement are provided in Table 1.

Table 1
Data collection and crystal structure refinement parameters for **1**.

Formula	$Fe_6Cl_2O_{7.66}N_{20}C_{48}H_{43.3}$ (**1**)
CCDC number	1832672
T (K)	100(2)
Molar mass (g/mol)	1428.81
Space group	$C2/c$
a (Å)	23.265(9)
b (Å)	11.918(4)
c (Å)	22.438(8)
β (°)	107.754(4)
V (Å^3)	5925.14
Z	4
Crystal color	Red
D_{calc} (g cm^{-3})	1.602
μ (mm^{-1})	1.588
λ (Å)	0.71073
$2\theta_{max}$ (°)	28.62
Total reflections	30239
R_{int}	0.074
Unique reflections	7116
Parameters refined	415
Restraints used	8
R_1, wR_2 [$I > 2\sigma(I)$][a]	0.086, 0.225
R_1, wR_2 (all data)	0.147, 0.258
Goodness-of-fit (GOF) on F^2[b]	1.042
Difference in peak/hole (e Å^{-3})	1.25, −1.10

[a] $R_1 = \Sigma||F_o| - |F_c||/\Sigma|F_o|$; $wR_2 = [\Sigma[w(F_o^2 - F_c^2)^2]/\Sigma[w(F_o^2)^2]]^{1/2}$.

[b] Goodness-of-fit = $[\Sigma[w(F_o^2 - F_c^2)^2]/(N_{obs} - N_{params})]^{1/2}$, based on all data.

2.1.3. Magnetic measurements

Magnetic properties of **1** were measured on a polycrystalline sample, using a superconducting quantum interference device (SQUID) magnetometer MPMS-XL (Quantum Design). Magnetic susceptibility was measured in a direct-current (DC) applied magnetic field of 0.1 T in the 1.8–300 K temperature range. The data were corrected for the diamagnetic contribution from the sample holder and for the intrinsic diamagnetism using tabulated constants [21].

2.1.4. Mössbauer spectroscopy

The zero-field, 80-K ^{57}Fe Mössbauer spectrum of **1** was recorded using a spectrometer operated in a constant acceleration mode. The instrument was equipped with a liquid nitrogen cooled cryostat. The sample consisted of ~50 mg of polycrystalline powder of **1** dispersed in eicosane and placed directly in a custom-made polyethylene cup closed with a lid. Isomer shifts were referenced against the centroid of a spectrum recorded at room temperature for a Fe metal foil.

2.1.5. Electrochemistry

Cyclic voltammetry (CV) was recorded on complex **1** dissolved in a 0.100 M solution of $(Bu_4N)PF_6$ in MeCN at room temperature. The measurements were performed using a 600D electrochemical analyzer (CH Instruments), at the sweep rate of 0.100 V·s^{-1}, with a Pt-disk working electrode, a Pt-wire counter electrode, and an Ag/AgCl reference electrode. All the potentials were referenced to the Fc^+/Fc couple (Fc = ferrocene), which was added as an internal standard upon completion of the CV experiment.

2.1.6. Theoretical calculations

Electronic structure calculations were performed at the density-functional theory (DFT) level using the GAUSSIAN 09

quantum-chemical software package [22]. An idealized (non-disordered) crystal structure of **1** determined by X-ray diffraction was used as the initial structural model. Single-point calculations and geometry optimizations were completed using standard convergence criteria and the B3LYP/6-311G functional/basis set combination. Geometry optimizations were performed for the $S = 15$ ferromagnetic (FM) state using both non-symmetrized (C_1) and symmetrized (C_{2h} and C_i) models (Fig. S1). Theoretical exchange coupling constants (J_{ij}) were predicted using the broken-symmetry (BS) formalism for both the experimental (X-ray) and optimized symmetrized geometries. The initial electronic guesses were obtained using the default guess option for the FM states and the *fragment* option of the *guess* keyword for the BS states. The non-zero J_{ij} values expected for the C_{2h} model were obtained by considering relative energies of the FM ($S = 15$) and of three distinct BS ($S = 5$) states of the [Fe^{III}_6] cluster. In this case the BS states were obtained by concomitantly flipping the spin for two distinct Fe sites (Fig. S2 and Tables S1–S2). In contrast, the J_{ij} values predicted for the experimental and optimized C_i (FM, $S = 15$) structures were obtained using the simpler [$Fe^{III}_2Ga^{III}_4$] models. Thus, the J_{ij} values were calculated from the difference between the energies of the FM and BS states using the relation $J = -\frac{E_{FM}-E_{BS}}{25}$, ($\hat{H}_{exchange} = -\sum_{i\neq j} 2J_{ij}\hat{\boldsymbol{S}}_i \cdot \hat{\boldsymbol{S}}_j$). For each J_{ij} constant, the specific *i*-*j* exchange interaction was "isolated" by replacing the other four paramagnetic high-spin Fe(III) ions with diamagnetic Ga(III) ions. This substitution is justified by the fact that these ions have similar ionic radii (0.64 vs. 0.62 Å, respectively, in the octahedral coordination [23]) and are known to substitute isomorphously. The character of a particular state was established by monitoring the predicted Mulliken atomic charges and spin densities. The predicted quadrupole splitting of Fe sites, ΔE_Q, was determined from the calculated electric field gradient (EFG) which was obtained using the standard *prop* keyword. The predicted isomer shifts were obtained using the calibration given by Vrajmasu et al. [24].

3. Results and discussion

3.1. Synthesis

The addition of $AgNO_2$ to the 1:4 mixture of $FeCl_2$ and 3-H_2bpp in methanol unavoidably resulted in the formation of hexanuclear complex **1**. The formation of such cluster could not be achieved to any significant extent by exposing the reaction mixture to air in the absence of $AgNO_2$. Therefore, we conclude that the formation of ferric cluster **1** is facilitated by oxidation of Fe(II) precursor by NO_2^- ions. We also observed the formation of a black precipitate, which is likely Ag_2O formed by exposure of precipitated AgCl to light (see the Materials and Methods section). The lack of any counter anions in the crystal structure, as described below, suggests that all Fe centers in complex **1** are in the +3 oxidation state. While a 1:1 ratio of $AgNO_2$ to $FeCl_2$ should be sufficient for one-electron oxidation of each Fe(II) ion, we observed that increasing the amount of $AgNO_2$ improved the overall yield of the product. Most likely, the reaction is facilitated by abstraction of Cl^- ions from the Fe(II) precursor, and thus the larger concentration of Ag^+ ions helps to shift the equilibrium toward the final product.

We note that an analogous complex was reported by Plaul et al. as a pyridine solvate, prepared by reacting $FeCl_2{\cdot}4H_2O$ with 3-H_2bpp in a 1:1 methanol/pyridine mixture under aerobic conditions with 70% yield [27]. In their procedure, pyridine served as the base necessary to deprotonate the 3-H_2bpp ligand while the Fe(II) ion was oxidized to the Fe(III) state by atmospheric oxygen.

3.1.1. Crystal structure

Complex **1** crystallizes in the monoclinic space group *C*2/*c*. The crystal structure of **1** features a hexanuclear ferric cluster, which can be viewed as composed of two trinuclear subunits (Fig. 1a). Each subunit contains a μ_3-oxide bridge centering the Fe_3 triangle. One of the Fe–Fe edges of the triangle (at the Fe–Fe distance of 2.972(2) Å) is supported by a μ_2-methoxide bridge while the other two edges (at the Fe–Fe distances of 3.456(3) and 3.511(3) Å) are spanned by μ_2-pyrazolato bridges. The combination of two trinuclear units related by an inversion center leads to an octahedral arrangement of Fe sites, each of which exhibits distorted octahedral coordination environment. The axial and equatorial Fe sites reside in the {N_4OCl} and {N_3O_3} ligand environments, respectively. The Fe–O and Fe–N bond lengths around all three Fe centers are comparable, varying from 1.924 to 2.036 Å and from 2.052 to 2.209 Å, respectively. The Fe–N distances to the pyridyl rings (2.205–2.209 Å) are notably longer than those to the pyrazolyl rings (2.052–2.180 Å). Overall, the observed bond lengths are similar to those observed in other high-spin Fe(III) complexes with {$Fe_3(\mu_3\text{-}O)$} fragments [1,7–8,25,26].

Cluster **1** is analogous to that reported by Plaul et al. [27], but in the latter case the complex crystalized as pyridine solvate in a chiral space group $P2_1$. In our case, we observe the presence of interstitial water and methanol molecules. In the course of the crystal structure refinement, it became obvious that one of the crystallographically unique μ_2-OMe^- bridges showed mixed occupancy with a μ_2-OH^- bridge. Introducing such disorder to the model resulted in much more meaningful crystal structure refinement parameters. The mixed occupancy in one of the bridges also

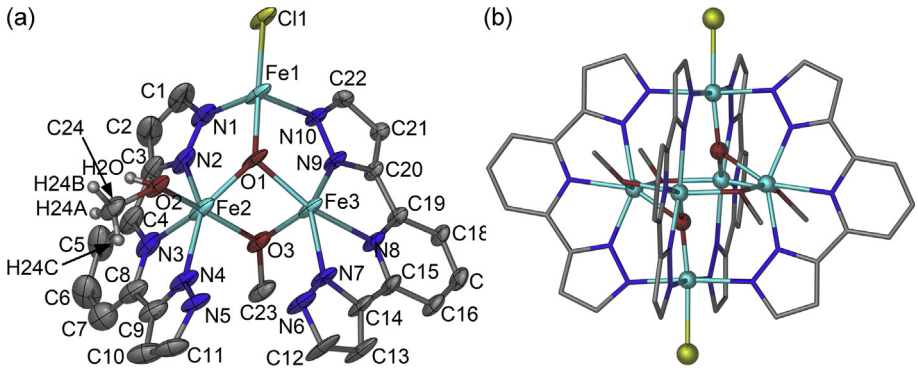

Fig. 1. (a) The asymmetric unit of **1**, with H atoms and interstitial solvent molecules omitted for clarity. Only H atoms that belong to the disordered μ_2-OMe/μ_2-OH bridge are shown. The thermal ellipsoids are shown at 35% probability level for better visualization. (b) The molecular structure of the hexanuclear complex, with H atoms and interstitial solvent molecules omitted for clarity. Selected interatomic distances (in Å): Fe1–Fe2 3.511(3), Fe1–Fe3 3.456(3), Fe2–Fe3 2.972(2), Fe1–Cl1 2.414(2), Fe1–O1 1.924(5), Fe1–N1 2.11(1), Fe1–N5 2.162(9), Fe1–N6 2.110(6), Fe1–N10 2.110(5), Fe2–O1 2.036(7), Fe2–O2 1.964(4), Fe2–O3 1.988(5), Fe2–N2 2.054(7), Fe2–N3 2.205(9), Fe2–N4 2.180(7), Fe3–O1 2.015(4), Fe3–O2 1.970(7), Fe3–O3 1.995(7), Fe3–N7 2.167(6), Fe3–N8 2.209(5), Fe3–N9 2.052(5).

correlated with the absence (if μ_2-OMe$^-$ was present) or presence (if μ_2-OH$^-$ was present) of a nearby interstitial methanol molecule, which is reflected in the final refined formula of complex **1**: $[Fe_6(\mu_3\text{-}3\text{-}bpp)_4(\mu_3\text{-}O)_2(\mu_2\text{-}OMe)_{3.67}(\mu_2\text{-}OH)_{0.33}Cl_2]\cdot 0.33MeOH\cdot H_2O$. The difference in the space group observed in our work as compared to the previous report might be explained by the ordered arrangement of these μ_2-OMe$^-$ and μ_2-OH$^-$ in the crystal structure refined by Plaul et al. [27]. Nevertheless, an analysis of our experimental X-ray diffraction data set revealed obvious systematic absences corresponding to the *C*-centered lattice with a *c*-glide plane, as well as the centrosymmetric nature of the lattice. Therefore, we preserved the *C*2/*c* space group initially suggested by XPREP [18].

3.1.2. Mössbauer spectroscopy

In order to unambiguously determine the oxidation and spin state of the Fe centers, a zero-field Mössbauer spectrum of **1** was recorded at 80 K. The experimental spectrum could be well modeled by two quadrupole doublets (Fig. 2), which have similar isomer shifts (0.496 and 0.488 mm/s) and linewidths (0.30 and 0.32 mm/s) but different quadrupole splitting parameters (0.946 and 0.378 mm/s). The 2:1 integrated intensity ratio of these doublets and the spectral parameters observed are consistent with the difference in the coordination environment between four equatorial and two axial ferric ions in cluster **1**. The smaller quadrupole splitting parameter observed for the axial Fe(III) sites suggests that they reside in a more symmetric coordination environment than those in the equatorial plane, which is consistent with the observed crystal structure (Fig. 1b).

3.1.3. Electrochemistry

The CV of complex **1** shows two quasi-reversible redox processes at $E_{1/2} = -0.24$ V and -0.57 V vs. Fc$^+$/Fc (Fig. 3). We attribute these two electrochemical events to successive one-electron reductions of the two $\{Fe_3(\mu_3\text{-}O)\}$ subunits observed in the crystal structure of this complex, thus leading in sequence to the formation of **1**$^-$ and **1**$^{2-}$ anions. Such reduction, which leads to delocalized $Fe^{3+/2+}$ mixed valence within each $\{Fe_3(\mu_3\text{-}O)\}$ triangle, has been recently demonstrated for a structurally related trinuclear Fe(III) complex [28]. The observation of well-separated redox processes suggests moderate electronic communication between the $\{Fe_3(\mu_3\text{-}O)\}$ subunits, and using $\Delta E_{1/2} = 0.33$ eV, one can estimate the equilibrium constant for comproportionation of the mixed-valent **1**$^-$ anion as being equal to 3.8×10^5.

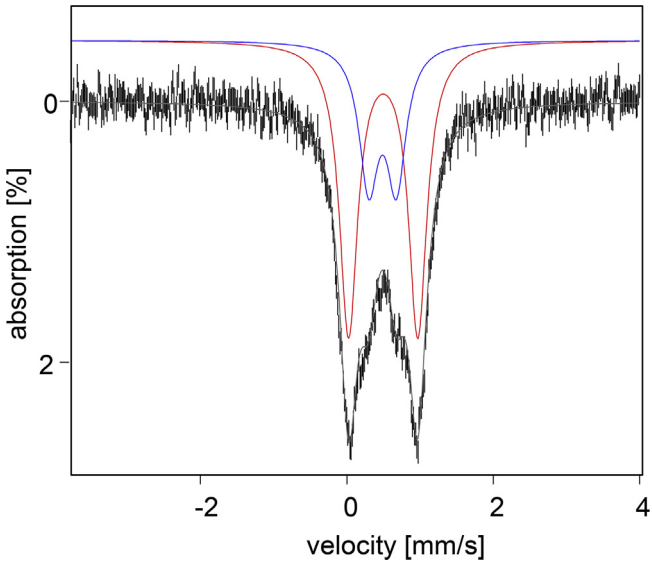

Fig. 2. Zero-field ^{57}Fe Mössbauer spectrum of **1** recorded at 80 K. The solid gray line is a simulation obtained by addition of two spectral components, which are shown with blue and red lines and offset from the experimental data for better visualization. (Color online.)

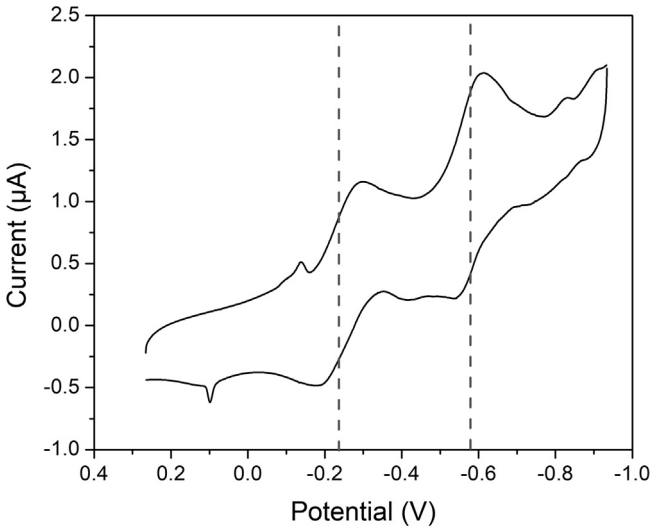

Fig. 3. Cyclic voltammogram of **1** recorded in a 0.1 M solution of $(Bu_4N)PF_6$ in MeCN. The vertical dashed lines indicate the $E_{1/2}$ values for the two redox couples observed for complex **1**.

3.1.4. Magnetic properties

Magnetic susceptibility measurements were performed on a ground polycrystalline sample of **1**. At 300 K, the value of χT is 8.75 emu mol^{-1} K, which is considerably lower than the value of 26.25 emu mol^{-1} K expected for six non-interacting high-spin Fe(III) centers. The χT value decreases nearly linearly as the temperature is lowered, approaching the value of 0 at low temperatures (Fig. 4a). The observed behavior suggests strong antiferromagnetic exchange between the Fe(III) centers in **1**, leading to an $S = 0$ ground state. The strong antiferromagnetic coupling is also evident in the nearly temperature-independent character of the magnetic susceptibility at higher temperatures (Fig. 4b). The increase in the value of χ at lower temperature is due to the presence of minor paramagnetic impurities not detectable in the Mössbauer experiment.

To rationalize the observed magnetic behavior of **1**, we turned to magneto-structural correlations and DFT calculations. The magnetism of this cluster is essentially determined by superexchange interactions between magnetically isotropic high-spin Fe(III) centers. These interactions are quantified by exchange coupling constants (J_{ij}) and can be rationalized considering the Fe-ligand bond lengths and the C_i molecular symmetry of the cluster. The presence of the inversion center results in 9 independent coupling constants out of 15 possible combinations for the hexanuclear cluster (Fig. 5a). These constants are $J_{12} = J_{36}$, $J_{13} = J_{26}$, $J_{14} = J_{56}$, $J_{15} = J_{46}$, $J_{24} = J_{35}$, $J_{25} = J_{34}$, $J_{16} = J_{23}$, and J_{45}, leading to the Heisenberg-Dirac-Van Vleck exchange Hamiltonian (1),

$$\begin{aligned}\hat{\mathbf{H}}_{C_i} = &-2J_{12}(\hat{\mathbf{S}}_1\cdot\hat{\mathbf{S}}_2+\hat{\mathbf{S}}_3\cdot\hat{\mathbf{S}}_6)-2J_{13}(\hat{\mathbf{S}}_1\cdot\hat{\mathbf{S}}_3+\hat{\mathbf{S}}_2\cdot\hat{\mathbf{S}}_6)\\&-2J_{14}(\hat{\mathbf{S}}_1\cdot\hat{\mathbf{S}}_4+\hat{\mathbf{S}}_5\cdot\hat{\mathbf{S}}_6)-2J_{15}(\hat{\mathbf{S}}_1\cdot\hat{\mathbf{S}}_5+\hat{\mathbf{S}}_4\cdot\hat{\mathbf{S}}_6)\\&-2J_{24}(\hat{\mathbf{S}}_2\cdot\hat{\mathbf{S}}_4+\hat{\mathbf{S}}_3\cdot\hat{\mathbf{S}}_5)-2J_{25}(\hat{\mathbf{S}}_2\cdot\hat{\mathbf{S}}_5+\hat{\mathbf{S}}_3\cdot\hat{\mathbf{S}}_4)\\&-2J_{16}(\hat{\mathbf{S}}_1\cdot\hat{\mathbf{S}}_6+\hat{\mathbf{S}}_2\cdot\hat{\mathbf{S}}_3)-2J_{45}\hat{\mathbf{S}}_4\cdot\hat{\mathbf{S}}_5\end{aligned} \quad (1)$$

This Hamiltonian can be further simplified by symmetrizing the structural model of **1** and by neglecting vanishing or small interactions. Thus, we assume that $J_{14} = J_{24} = J_{35} = J_{56} = J$, $J_{12} = J_{36} = j$,

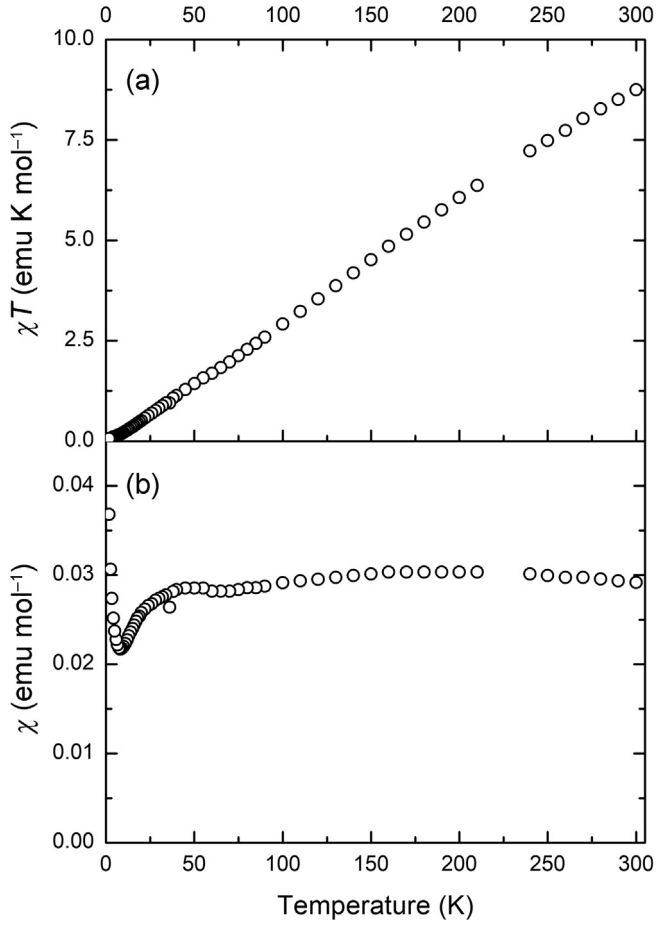

Fig. 4. Temperature dependences of χT (a) and χ (b) for a polycrystalline sample of **1**.

$J_{13} = J_{26} = j'$, and $J_{16} = J_{23} = J_{45} = 0$, which leads to a Hamiltonian that only requires three distinct exchange coupling constants:

$$\hat{\mathbf{H}}_{C_{2h}} = -2J(\hat{\mathbf{S}}_1 \cdot \hat{\mathbf{S}}_4 + \hat{\mathbf{S}}_2 \cdot \hat{\mathbf{S}}_4 + \hat{\mathbf{S}}_3 \cdot \hat{\mathbf{S}}_5 + \hat{\mathbf{S}}_5 \cdot \hat{\mathbf{S}}_6) - 2j(\hat{\mathbf{S}}_1 \cdot \hat{\mathbf{S}}_2 + \hat{\mathbf{S}}_3 \cdot \hat{\mathbf{S}}_6) - 2j'(\hat{\mathbf{S}}_1 \cdot \hat{\mathbf{S}}_3 + \hat{\mathbf{S}}_2 \cdot \hat{\mathbf{S}}_6), \quad (2)$$

We expect the strongest superexchange interactions to take place between the Fe sites bridged by the μ_3-oxo ligands. The presence of two trinuclear subunits, each centered around a μ_3-O^{2-} ligand with short Fe–O bonds (1.924 Å for the axial Fe sites and 2.015 and 2.036 Å for the equatorial ones), suggests the exchange interactions within the subunits are dominant and the magnetic properties of **1** are only weakly modulated by the exchange interactions between the subunits. Although the cluster core of **1** is supported by ligands other than carboxylates, we used the magneto-structural correlations proposed by Gorun and Lippard [1], Weihe and Güdel [29], and Mitchell and Christou [7] to obtain an empirical estimate of the exchange coupling constants in Eq. (2). As shown in Table 2, these expressions predict that the μ_3-O-linked Fe(III) sites exhibit relatively strong superexchange interactions. These correlations, however, also predict an unexpectedly strong inter-trimer interaction mediated by two equatorial μ_3-OMe^- ligands.

To obtain a better theoretical estimate of the coupling constants we turned to broken-symmetry (BS) DFT calculations at the B3LYP/6-311G level of theory. For these calculations we employed unabridged structures of symmetrized (C_{2h} and C_i) and experimental X-ray based models (Fig. S1 and Table S4). The J, j, and j' constants in Eq. (2) quantify the only interactions expected to be non-zero for the C_{2h} model of **1**. These parameters were estimated using a [Fe^{III}_6] computational model (Tables S1–S2). In contrast, the J_{ij} parameters of Eq. (1), expected for the C_i model (whether based on the experimental X-ray or geometry-optimized structures), were obtained using a series of simpler, [$Fe^{III}_2Ga^{III}_4$] models. In this case, four selected $S = 5/2$ Fe(III) sites were replaced by diamagnetic Ga (III) ions. The validity of the DFT-predicted electronic structures was assessed by comparing the theoretical zero-field Mössbauer parameters with those experimentally observed (Table S3). These calculations suggest that, as expected, μ_3-O-mediated interactions are dominant. They lead to a $S = 5/2$ ground state for each trinuclear subunit of cluster **1**. These subunits involve sites Fe1, Fe2, Fe4 and Fe3, Fe5, Fe6 (Fig. 5a). Antiferromagnetic exchange between the trinuclear subunits leads to the total ground state of $S = 0$. Assessing the nature and energies of the excited states requires either the diagonalization of a $6^6 \times 6^6 = 46656 \times 46656$ matrix or the use of irreducible tensor operators (ITO) approach.

Shown in Fig. 5b is the calculated spin configuration, which is expected to provide the dominant contribution to the ground state. The exchange interactions shown in purple and blue enforce an

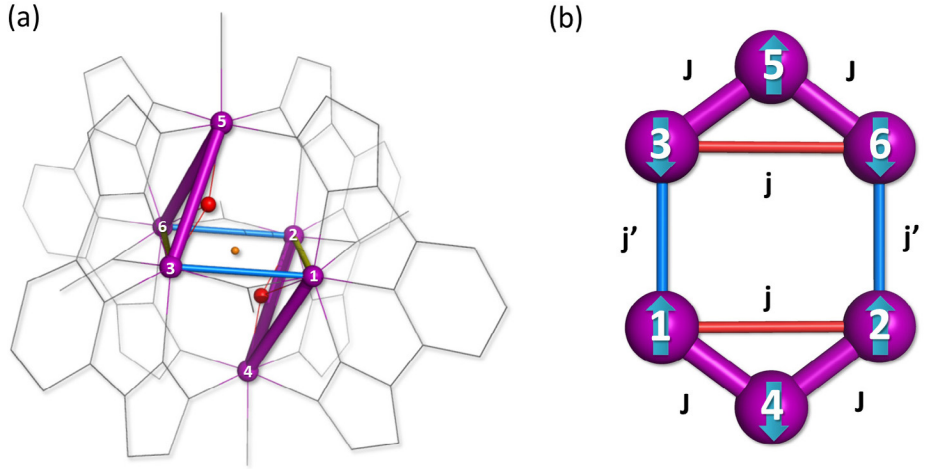

Fig. 5. (a) The relative magnitudes of DFT-predicted exchange interactions overlaid on the molecular frame, along with the numbering scheme used in the analysis of the exchange coupling constants in complex **1**. The inversion center is shown in orange and the bridging μ_3-O^- ligands are shown as red spheres. The strongest interactions are shown in purple, $J \sim -33$ cm^{-1}, followed by those in blue, $j \sim -12$ cm^{-1}, and in yellow, $j' = -5$ cm^{-1}. (b) DFT-predicted spin configuration that is expected to provide the dominant contribution to the ground state.

Table 2
Magnetic exchange constants obtained from single-point DFT calculations on the X-ray crystal structure of complex **1**.

Sym. J_{ij}	Empirical[a] J_{ij}, cm^{-1}			DFT, C_i				DFT, C_{2h}	
				$E_{FM} - E_{BS}$, cm^{-1}		J_{ij}, cm^{-1}		Constant	J_{ij}, cm^{-1}
	G-L[a]	W-G[b]	M-C[c]	X-ray	Opt.	X-ray	Opt.		
$J_{14} = J_{56}$	−11	−26	−16	816	676	−33	−27	J	−24
$J_{24} = J_{35}$	−13	−29	−17	832	679	−33	−27		
$J_{12} = J_{36}$	−10	−32	−6	116	96	−5	−4	j	−8
$J_{13} = J_{26}$	−13	−33	−14	312	230	−12	−9	j'	
$J_{15} = J_{46}$	0	0	0	6	−13	0	1	N/A	
$J_{25} = J_{34}$	0	0	0	−11	−15	0	1		
J_{16}	0	0	0	167	141	−7	−6		
J_{23}	0	0	0	83	143	−3	−6		
J_{45}		N/A			50		−2		

[a] Empirical values J_{ij} obtained using the Gorun-Lippard expression [1], $J = -8.763 \times 10^{11} \times exp(-12.663r)$, where r represents half of the shortest superexchange pathway.
[b] Empirical values J_{ij} obtained using the Weihe-Güdel's expression [29], $J = -0.668 \times 10^{8} \times (3.536 + 2.488cos\phi + cos^2\phi)exp(-7.909r)$, where r is the mean Fe–O bond length and ϕ is the Fe–O–Fe bond angle.
[c] Empirical values J_{ij} obtained using the Mitchell-Christou expression [7], $J = -1.23 \times 10^{9} \times (-0.12 + 1.57cos\phi + cos^2\phi)exp(-8.99r)$, where r is the mean Fe–O bond length and ϕ is the Fe–O–Fe bond angle.

antiparallel alignment of the interacting spins. Therefore, these interactions lead to the stabilization of the total $S = 0$ ground state. In contrast, the interactions highlighted in red introduce spin frustration and thus destabilize the ground state.

4. Conclusion

In summary, the intentional oxidation of Fe(II) ions by $AgNO_2$ in the presence of the tridentate ligand 3-H_2bpp leads to $[Fe_6(\mu_3\text{-}3\text{-bpp})_4(\mu_3\text{-O})_2(\mu_2\text{-OMe})_{3.67}(\mu_2\text{-OH})_{0.33}Cl_2]\cdot 0.33MeOH\cdot H_2O$ (**1**), a ferric complex with a hexanuclear cluster core. The structure of this complex can be viewed as composed of two symmetry-related trinuclear subunits, each centered by a μ_3-oxo linker. Consequently, strong antiferromagnetic exchange is observed within these subunits, which leads to spin frustration. The interaction between the subunits is also antiferromagnetic in nature, thus resulting in the total $S = 0$ ground state. Mössbauer spectroscopy performed on complex **1** confirmed the presence of Fe(III) sites with distinctly different coordination environments in the 2:1 ratio.

Acknowledgments

The National Science Foundation is gratefully acknowledged for the support of this research (award CHE-1464955 to M.S.). S.A.S. acknowledges the support of the University of Idaho. The Mössbauer data were obtained at the National High Magnetic Field Laboratory (NHMFL), which is supported by the NSF Cooperative Agreement (DMR-1157490) and the State of Florida. This work used the Extreme Science and Engineering Discovery Environment (XSEDE), which is supported by NSF grant ACI-1548562.

Appendix A. Supplementary data

Supplementary data associated with this article can be found, in the online version, at https://doi.org/10.1016/j.poly.2018.06.004.

References

[1] (a) S.M. Gorun, S.J. Lippard, Inorg. Chem. 30 (1991) 1625;
(b) E.M. Rumberger, S. Hill, R.S. Edwards, W. Wernsdorfer, L.N. Zakharov, A.L. Rheingold, G. Christou, D.N. Hendrickson, Polyhedron 22 (2003) 1865.
[2] E.M. Rumberger, S. Hill, R.S. Edwards, W. Wernsdorfer, L.N. Zakharov, A.L. Rheingold, G. Christou, D.N. Hendrickson, Polyhedron 22 (2003) 1865.
[3] J.D. Compain, P. Mialane, A. Dolbecq, I.M. Mbomekallé, J. Marrot, F. Sécheresse, E. Rivière, G. Rogez, W. Wernsdorfer, Angew. Chem., Int. Ed. 48 (2009) 3077.
[4] D. Gatteschi, R. Sessoli, A. Cornia, Chem. Commun. (2000) 725.
[5] E.Y. Tshuva, S.J. Lippard, Chem. Rev. 104 (2004) 987.
[6] J.J. Phillips, J.E. Peralta, G. Christou, J. Chem. Theory Comput. 9 (2013) 5585.
[7] K.J. Mitchell, K.A. Abboud, G. Christou, Inorg. Chem. 55 (2016) 6597.
[8] C. Cañada-Vilalta, T.A. O'Brien, E.K. Brechin, M. Pink, E.R. Davidson, G. Christou, Inorg. Chem. 43 (2004) 5505.
[9] H.A. Goodwin, Top. Curr. Chem. 233 (2004) 59.
[10] M.A. Halcrow, Polyhedron 26 (2007) 3523.
[11] H. Phan, J.J. Hrudka, D. Igimbayeva, L.M. Lawson Daku, M. Shatruk, J. Am. Chem. Soc. 139 (2017) 6437.
[12] M. Shatruk, H. Phan, B.A. Chrisostomo, A. Suleimenova, Coord. Chem. Rev. 289 (2015) 62.
[13] D. Fedaoui, Y. Bouhadja, A. Kaiba, P. Guionneau, J.F. Létard, P. Rosa, Eur. J. Inorg. Chem. (2008) 1022.
[14] H.J. Shepherd Kaiba, D. Fedaoui, P. Rosa, A.E. Goeta, N. Rebbani, J.F. Létard, P. Guionneau, Dalton Trans. 39 (2010) 2910.
[15] K.H. Sugiyarto, W.A. McHale, D.C. Craig, A.D. Rae, M.L. Scudder, H.A. Goodwin, Dalton Trans. (2003) 2443.
[16] P. Gamez, R.H. Steensma, W.L. Driessen, J. Reedijk, Inorg. Chim. Acta 333 (2002) 51.
[17] SMART and SAINT, Bruker AXS Inc., Madison, WI, USA, 2007.
[18] G.M. Sheldrick, SADABS, University of Gottingen, Gottingen, Germany, 1996.
[19] G.M. Sheldrick, XPREP. Space group determination and reciprocal space plots, Siemens Analytical X-ray Instruments, Madison, WI, USA, 1991.
[20] G.M. Sheldrick, Acta Crystallogr. Sect. A A64 (2008) 112.
[21] G.A. Bain, J.F. Berry, J. Chem. Educ. 85 (2008) 532.
[22] M.J. Frisch, G.W. Trucks, H.B. Schlegel, G.E. Scuseria, M.A. Robb, J.R. Cheeseman, G. Scalmani, V. Barone, B. Mennucci, G.A. Petersson, et al., Gaussian 09, Revision D.01, Gaussian Inc., Wallingford, CT, 2009.
[23] R.D. Shannon, Acta Crystallogr. Sect. A 32 (1976) 751.
[24] V. Vrajmasu, E. Münck, E.L. Bominaar, Inorg. Chem. 42 (2003) 5974.
[25] D. Piñero, P. Baran, R. Boca, R. Herchel, M. Klein, R.G. Raptis, F. Renz, Y. Sanakis, Inorg. Chem. 46 (2007) 10981.
[26] W.M.C. Sameera, D.M. Piñero, R. Herchel, Y. Sanakis, J.E. McGrady, R.G. Raptis, E.M. Zueva, Eur. J. Inorg. Chem. 2012 (2012) 3500.
[27] D. Plaul, T. Spielberg Eike, W. Plass, Z. Anorg. Allg. Chem. 636 (2010) 1268.
[28] E.V. Govor, K. Al-Ameed, I. Chakraborty, C.S. Coste, O. Govor, Y. Sanakis, J.E. McGrady, R.G. Raptis, Angew. Chem., Int. Ed. 56 (2017) 582.
[29] H. Weihe, H.U. Güdel, J. Am. Chem. Soc. 119 (1997) 6539.